Ceramics International 50 (2024) 684–691

Contents lists available at ScienceDirect

Ceramics International

journal homepage: www.elsevier.com/locate/ceramint

Innovative low-critical raw materials and medium-entropy perovskite for intermediate temperature solid oxide electrochemical cells

Sebastian Vecino-Mantilla [a], Gaetano Squadrito [a], Fabio Torazzi [b], Vincenzo M. Sglavo [b], Massimiliano Lo Faro [a,*]

[a] Institute of Advanced Energy Technologies (ITAE) of the Italian National Research Council (CNR), Via Salita S. Lucia sopra Contesse 5, 98126, Messina, Italy
[b] Dipartimento di Ingegneria Industriali, Università di Trento, Via Sommarive 9, 38123, Trento, Italy

ARTICLE INFO

Handling Editor: Dr P. Vincenzini

Keywords:
Green deal
Perovskite
Electrochemistry
Gas-to-power
Power-to-gas
REPowerEU

ABSTRACT

Ceramic proton conductive electrolytes are promising materials for reducing the operating temperatures of solid oxide cells. It is desirable to achieve such a target because, as a result, durability, cost of materials, electrochemical reactions and flexibility of its use can be significantly enhanced. A medium-entropy perovskite with the stoichiometric formula $Ba_{0.5}Sr_{0.5}Zr_{0.5}Zn_{0.5}O_3$ was studied in the present work using limited amounts of critical raw materials. According to the performed analysis, it is possible to achieve complete phase purity at 1300 °C. Based on dilatometric measurements, the material can undergo significant densification starting at 1200 °C; at about 1550 °C the produced perovskite melts and degrades simultaneously. One of the most effective characteristics of the pure phase is its ability to absorb moisture and the excellent stability to redox mechanism. This material's characteristic was confirmed by a series of thermochemical procedures and XRD analyses. As a result of electrochemical measurements carried out on 93% dense pellet consolidated at 1350 °C, the material has a much better conductivity and activation energy than BZY.

1. Introduction

One of the most current and debated problems in the world consists in finding a technological asset which could at the same time decrease the carbon foot-print and improve the use of non-critical resources [1–5]. It is almost clear that this requires a step change in the use and transport of energy as well as in circular economy based on energetic resources and raw material easily available [6,7]. Along this path, the most advanced countries are looking at hydrogen as energy vector for such transition [8,9].

Concerning the technologies, it is almost evident that to produce H_2, as well as for its transformation to synthetic chemical or power energy generation, the electrochemical cells are the most promising devices considering the involved reaction mechanisms [10–13]. Therefore, the efficiency depends only on the thermodynamics of the involved reactions and the internal resistances that could be reduced with intense research studies.

The use of critical raw materials (CRM) is also an issue at least at the same level of the prior said challenge concerning the development of more advanced electrochemical devices. As for this aspect, one possible technology achieving both targets is that based on solid oxide electrochemical cells [14]. Such devices have already demonstrated superior efficiency although some limitations are still present in their application [15–17]. Most of these restrictions derives from the high operating temperatures which can not be lower than 650 °C for the most advanced cells to achieve appropriate performances [18]. Such limitations could be surpassed by the introduction of novel materials especially regarding the electrolyte, which represents the most intensive constraint for the efficiency of cells, its behaviour involving the transport of ions which requires more energy than the transport of electrons [19,20].

In conventional ceramic electrolytes, the species involved in current transport are oxygen ions which require high energy to be efficiently mobile [21–25]. Typically, these ions require an energy higher than 0.9 eV and therefore the practical approach consist in reducing the thickness of the electrolyte below 10 μm in order to achieve a compromise between performance and operating temperature. Another possibility is related to the development of ceramic electrolyte characterized by proton conductivity [26–29]. With respect to oxygen ions, protons require lower energy to diffuse; depending on the involved mechanism they can require from less than 10 eV like in polymeric electrolyte to

* Corresponding author.
E-mail address: lofaro@itae.cnr.it (M. Lo Faro).

https://doi.org/10.1016/j.ceramint.2023.10.146
Received 9 August 2023; Received in revised form 2 October 2023; Accepted 16 October 2023
Available online 17 October 2023

approximately 30 eV in the already demonstrated ceramic perovskites where protons are transported as a consequence of the oxygen vacancies hydration [30]. Zirconate and cerate are the class of perovskites currently under studies for such uses [31–34]. However, both have still some limitations. For example, zirconates have shown very interesting proton conductivity, but they require temperatures higher than 1600 °C for achieving a proper densification [35–37]. Such temperatures are not optimal for the manufacture of currently used anode supporting cells. On the other hand, cerates could be densified at temperatures around 1400 °C but their conductivity is lower and they show quite marked alkaline behaviour, which represents an issue for the thermal treatment and the operating conditions since the presence of CO_2 promotes the formation of insulating carbonates [38–40]. Therefore, research is quite active in this field to find proper doping or alternative compositions. Due to these premises, high entropy oxides are worth to be investigated due to their advanced mechanical, thermal, and chemical properties relevant for their use in electrochemical devices [41–43].

The present research activity aimed at examining a $Ba_{0.5}Sr_{0.5}Zr_{0.5}Zn_{0.5}O_3$ (BSZZ) perovskite with maximum entropy. This formulation was developed to minimize the use of critical raw materials and to find a composition stable into a cubic phase within Goldsmith's tolerance [44]. Cerium is currently included in the list of such materials and therefore the perovskite was formulated using the properties of zirconates in combination with the potentialities guaranteed by zinc.

There is no doubt that zirconates, when doped with various cations, have enticing properties and could offer a platform for the addition of further cations. On the other hand, there is still controversy regarding the influence of Zn on perovskites. Zinc was generally recommended at low percentage (*i.e.,* 0.5–5 wt%) as sintering aid for achieving proper densification at practical temperatures [45,46]. While suggesting ZnO as a sintering aid, it was also reported that this element may contribute to undesired electronic leakage [47–49]. Conversely, some studies have reported that it is strongly desired in materials used as electrolytes for proton carrier exchange because of its powerful and positive role as proton uptake [50–55]. In addition, the high entropy could ensure a stable material with novel properties. This aspect was often addressed by including a large number of cations within the perovskite [41,43]. However, this approach has had marginal practical utility due to the high risk of secondary phases and lack of understanding of individual cation role.

These considerations prompted us to carry out a detailed study of BSZZ perovskite prepared by the modified-Pechini method [56,57]. The results of comprehensive physico-chemical and electrochemical characterizations of this novel material are presented here with the goal to examine BSZZ as a promising electrolyte or as a platform for further inclusion of cations to increase its entropy.

2. Materials and methods

The modified-Pechini method for the synthesis of $Ba_{0.5}Sr_{0.5}Zr_{0.5}Zn_{0.5}O_3$ (*i.e.,* BSZZ) required stoichiometric amounts of Ba-, Sr-, Zr-, and Zn- salts dissolved in distilled water. The following ones were used: $ZrO(NO_3)_2{\cdot}xH_2O$ (99%, Aldrich), $Zn(NO_3)_2{\cdot}6H_2O$ (98%, Sigma-Aldrich), $Sr(NO_3)_2$ (99%, Aldrich), $Ba(NO_3)_2$ (99.999%, Aldrich). During constant stirring, the salt solution was heated to 120 °C and then an ammonia solution (28–30%, Supelco) was added. The solution was then gelled with EDTA (99.995%, Aldrich) once it reached 150 °C. The organics were then removed from the gel by drying and annealing at 200 °C (3 h), 500 °C (3 h), and 800 °C (3 h). The powder was ground and pelletized in a ball mill and then thermally treated at 1000–1300 °C to determine the temperature necessary for obtaining a single-phase formation. After each thermal treatment carried out for 6 h, XRD analysis was performed with a Bruker D8 ADVANCE diffractometer operating at 40 kV and 40 mA. BSZZ with acceptable crystallinity was then subjected to physical and structural studies including dilatometric and SEM/EDXS analyses. Dilatometry was carried out using a pellet of 6 mm diameter/0.9 mm thickness made from powder calcined at 800 °C and uniaxially pressed at 350 MPa. This analysis was carried out in air with a horizontal LINSEIS L75 PLATINUM SERIES instrument equipped with alumina piston, tube and spacers. The heating/cooling rate was 5 °C min^{-1} from room temperature up to 1550 °C with 1 h dwell time. The specimen was observed by Scanning Electron Microscope (SEM, Jeol JSM 5500) equipped with Energy Dispersion X-ray Spectroscopy probe (EDXS, EDS2000; IXRF System) after being coated with thin Pt–Pd layer by sputtering.

ALTAMIRA AMI-300 instrument was used to study the redox properties of optimised BSZZ powders. The material was subjected to a first cycle of reduction (TPR), post-oxidation (TPO) and second reduction (TPR) at 900 °C in Ar with 5 vol% H_2 or 5 vol% O_2. A preliminary degassing process was required (Ar 38 cm^3 min^{-1} was heated from room temperature to 300 °C at a rate of 10 °C min^{-1}, followed by 20 min dwell time and cooling down to room temperature). Afterwards, thermal analyses were conducted with dwell time of 20 min at 10 °C min^{-1}. For an optimal reduction profile, we set the empiric numbers K ($55 < K < 150$ in s) and P ($20 < P < 50$ in °C) defined by Monti et al. [58]. As a follow-up of these analyses, XRD scans were carried out to determine possible structure modifications. Further analyses included the evaluation of the structure after treatment under humidified H_2 up to 900 °C.

The electrical behaviour of BSZZ was then studied. The raw powder obtained after calcination at 800 °C was pelletized and thermally treated at 1350 °C for 12 h. Electrochemical tests were performed to determine conductivity. As a preliminary step, gold contacts were deposited on both sides of a pellet with thickness of 337 μm (determined by SEM analysis after the test). Gold coated electrolyte was mounted on a test bench purchased from Advanced Measurements. This set up consists of two opposite alumina tubes blocking the electrolyte with controlled force. Dry or wet gases can flow through these tubes. Moreover, gold contacts located within the alumina tubes are connected to four gold wires for measuring potentials and currents. Electrochemical measurements were carried out with BioLogic equipment and involved impedance spectroscopies (EIS) at temperatures ranging from 200 to 800 °C in the presence of humidified H_2. Series resistance was determined by the intercept of EIS spectrum at high frequency with x-axis, and then an Arrhenius plot was extrapolated using pellet conductivity whereas the activation energy was determined using the Boltzmann equation. SEM FEI XL 30 was used to examine the morphology of the spent electrolyte.

The surface structure of BSZZ was analysed using a PHI 5800-01 spectrometer equipped with a monochromatic Al Kα X-ray source (XPS). In addition to using the native software of the instrument to analyse the XPS spectra, the bands were assigned using data from the literature and the NIST X-ray Photoelectron Spectroscopy Database.

3. Results

The XRD spectra of BSZZ after a series of thermal treatments are shown in Fig. 1. Perovskites is poorly present at 1000 °C, while several phases mainly corresponding to the constituting oxides are identified. When the material is heated to 1100 °C, two-three phases begin to form, improving the material structure. One of these is clearly associated with ZnO (COD 2107059). Impurities corresponding to about 6% Zr suboxide are present up to 1250 °C, as clearly visible along the shoulder of the narrow peak at 30° and along the broad peak at 38.5°. At 1300 °C, the desired phase was definitively achieved with a purity matching COD card 1521389. As determined by the Scherrer equation, the crystallites size is 38 nm. The obtained phase has a cubic structure corresponding to the Patterson Space Group Pm-3m, with $a = b = c$ parameters equal to 4.160119 Å, unit cell volume of 71.997 $Å^3$ and theoretical density of 5.41 g cm^{-3}. In addition, since Zr-suboxides are completely incorporated at temperatures over 1300 °C, the peak around 30° is shifted to 30.4° (see inset of Fig. 1).

The dilatometric analysis is shown in Fig. 2; the derivative of the deformation vs. temperature is also shown to highlight better the

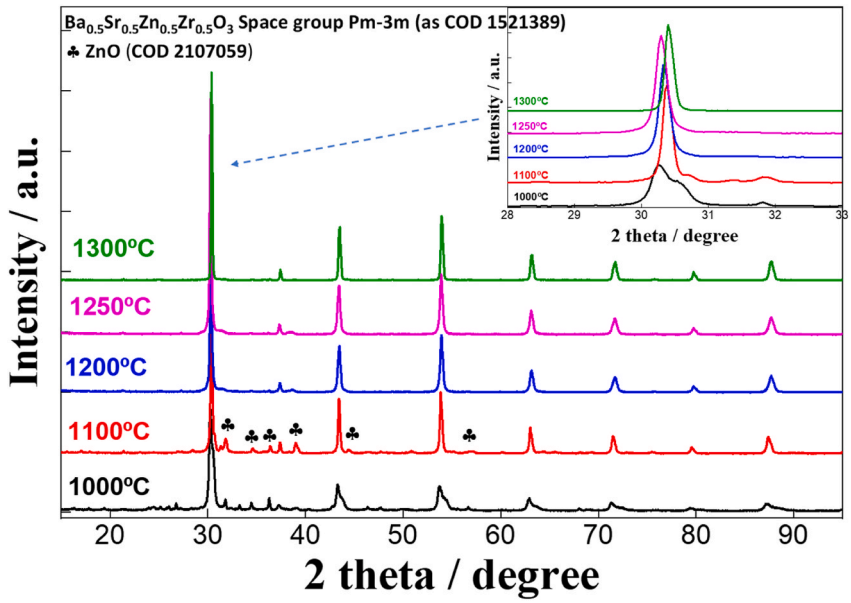

Fig. 1. XRD analysis of BSZZ following thermal treatments in the range of 1000–1300 °C. The inset reports the magnification of peak around 30° showing the effect of temperature on (101) reflection peak.

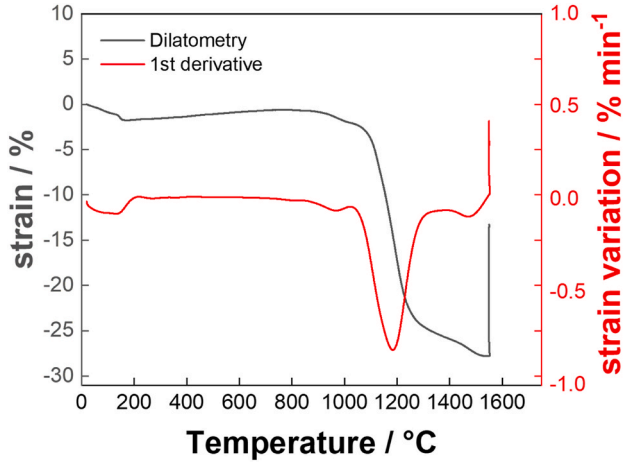

Fig. 2. Dilatometric profile of BSZZ pellet made from powder calcined at 800 °C.

evolution of the material. At about 100–150 °C a limited shrinkage is recorded very likely due to the loss of humidity this powder could have acquired during the manipulation and storage. Two significant although limited shrinkages are then observed at 855 °C and 965 °C. The undulations in the signal may indicate a rearrangement of the structure that results in the main phase and multiple impurities observed for the sample calcined at 1000 °C (Fig. 1). Above 1050 °C the real densification takes place whose maximum intensity is around 1180 °C. During the isotherm at 1550 °C the material decomposes and melts. SEM/EDXS analyses point out the formation of a liquid phase where the different oxides (especially zinc and zirconium oxides) solidify separately upon cooling.

As a means of studying BSZZ's redox stability, we performed a cyclic thermal analysis consisting of a first programmed reduction (1st TPR), post-thermal programmed oxidation (TPO) and a second programmed reduction (2nd TPR). The samples were then analysed by XRD. Fig. 3 shows the thermal analysis profiles. A very weak enhancement of thermal conductivity detector (TCD) signal was observed during the first TPR, making the baseline slightly higher. A small event occurs around

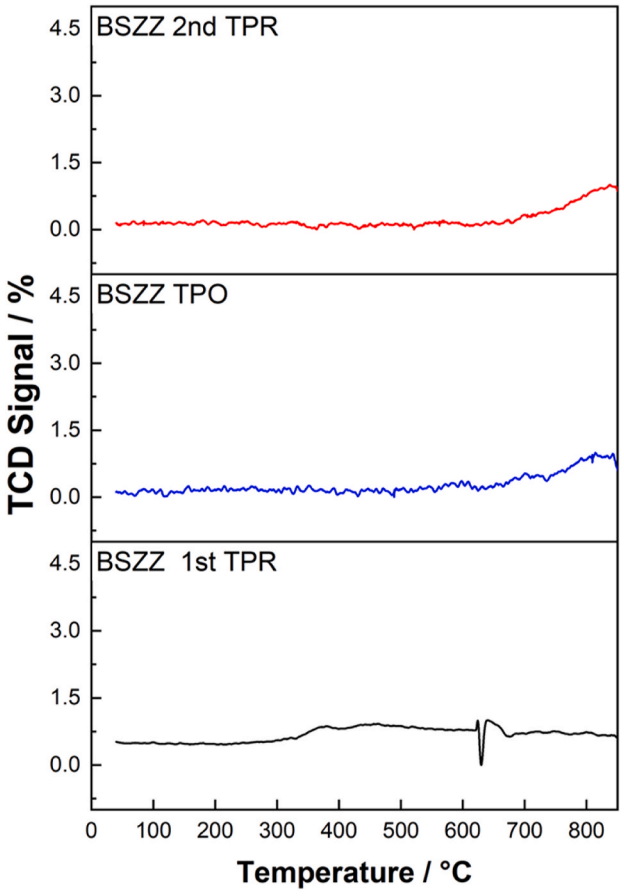

Fig. 3. Profiles of thermal analyses that were carried out in the order of 1st TPR, TPO, and 2nd TPR.

350 °C. Around 630 °C, a spike is identified with an intensity and feature similar to events not directly related to material reduction. However, the relative variation is around 0.75 % compared to the baseline. Accordingly, this first reduction procedure shows no significant features for

BSZZ. As a result of the programmed oxidation test (TPO), this thermal analysis detected only a very tiny signal, less than 1%, at around 650 °C. Also in this case, this broad signal remained negligible. Similar to the previous TPO, the second TPR shows a broad band starting around 680 °C, with a relative variation of approximately 1%. It is possible that some equipment limitations could be responsible for the similarity between the TPO and 2nd TPR profiles because of changes in the thermal conductivity of the gases used for these analyses. Therefore, as mentioned before, we collected XRD profiles at each step of analysis to gain a better understanding of the material's behaviour.

The XRD patterns of the specimens after programmed oxidations/reductions thermal treatments are shown in Fig. 4. Apart from the redox cycles described above, the BSZZ powder was also re-heated to 1300 °C for 2 h and then to 800 °C in the presence of humidified O_2 for 6 h. According to Fig. 4a, the material structure remains essentially unchanged during thermal treatment and no new phases are observed because of redox cycles and humidity. By examining the peak around 30° in Fig. 4b, additional information can be collected. Since the redox cycles does not affect the structure of the materials, it can be assumed that the broad and weak signals observed in the thermal treatment profiles in Fig. 3 were not significant. In fact, the peaks are clearly centred around 30.4015°, and the broadening of this peak is essentially unchanged. In the sample treated with humidification, this peak moves at a lower angle of about 0.03°, which agrees with the uptake of proton in BSZZ crystal structure. A similar behaviour was observed by Wang et al. in their study related to mobile carriers for protonic ceramic conductors [59].

For the conductivity measurement, the powder calcined at 800 °C was ball milled, pressed and thermally treated at 1350 °C. An XRD analysis of BSZZ was performed prior to electrochemical measurements to ensure that no secondary phases were formed as a result of the thermal treatment. As shown in Fig. 5a, the electrolyte maintains excellent phase purity with an average crystal size of approximately 55 nm. At different magnifications, Fig. 5b and c shows that the pellet achieves appreciable densification. On the basis of density measurements and the theoretical density of BSZZ equal 5.41 g cm^{-3}, it can be estimated that the pellet was 92.7% dense. The treatment at 1350 °C was found to be the most effective compromise to achieve a dense material and avoid the formation of cracks or decompositions and promising results were obtained by carrying out electrochemical measurements.

The Arrhenius plot in Fig. 6 was determined by combining EIS data of BSZZ studied in humidified hydrogen. Specifically, the Arrhenius graph for BSZZ was determined by plotting the series resistance (intercept at high frequency, x-axis) for EIS spectra collected between 250 and 800 °C at 50 °C intervals. The data concerning one of the most common proton conductive ceramics, $BaZr_{0.8}Y_{0.2}O_{3-d}$ (BZY) from Chen et al. recent paper are also plotted in Fig. 6 [33] studied under similar conditions to those adopted for the BSZZ. According to Fig. 6, at all the investigated temperatures, BSZZ exhibits higher conductivity than BZY. In Fig. 6, BSZZ conductivity shows two distinct slopes, indicating that there is a significant change in the conductivity mechanism. It is well known that proton conductive ceramics do not contain proton species. Consequently, external humidification is required to provide proton species. The degree of humidification of ceramic oxygen vacancies determines the number of proton species available for transport. In general, the formation of such charged species is described by the following equation in the Kröger-Vink notation:

$$H_2O + V_o^{\cdot\cdot} + O_o^{\times} \leftrightarrow 2OH_o^{\cdot} \qquad \text{equation 1}$$

An electrical potential can then cause proton migration at the intrinsic defect level according to a hopping (Grotthuss) mechanism [60]. It is evident that for such mechanism to be effective, a proton conductive ceramic must have a high degree of hydration. Ideally, such material should be saturated. A similar event, however, depends on the operating conditions, including the provided amount of water and the operating temperature. However, at certain high temperatures, humidification of ceramic defects becomes impossible, turning the conductive mechanism into the traditional one based on oxygen ions. Thus, the different trends shown by the experimental data must be explained by a change in the transport mechanism and related activation energy. Because protons require less energy to diffuse than oxygen ions, their conduction can be more effective at lower temperatures. According to

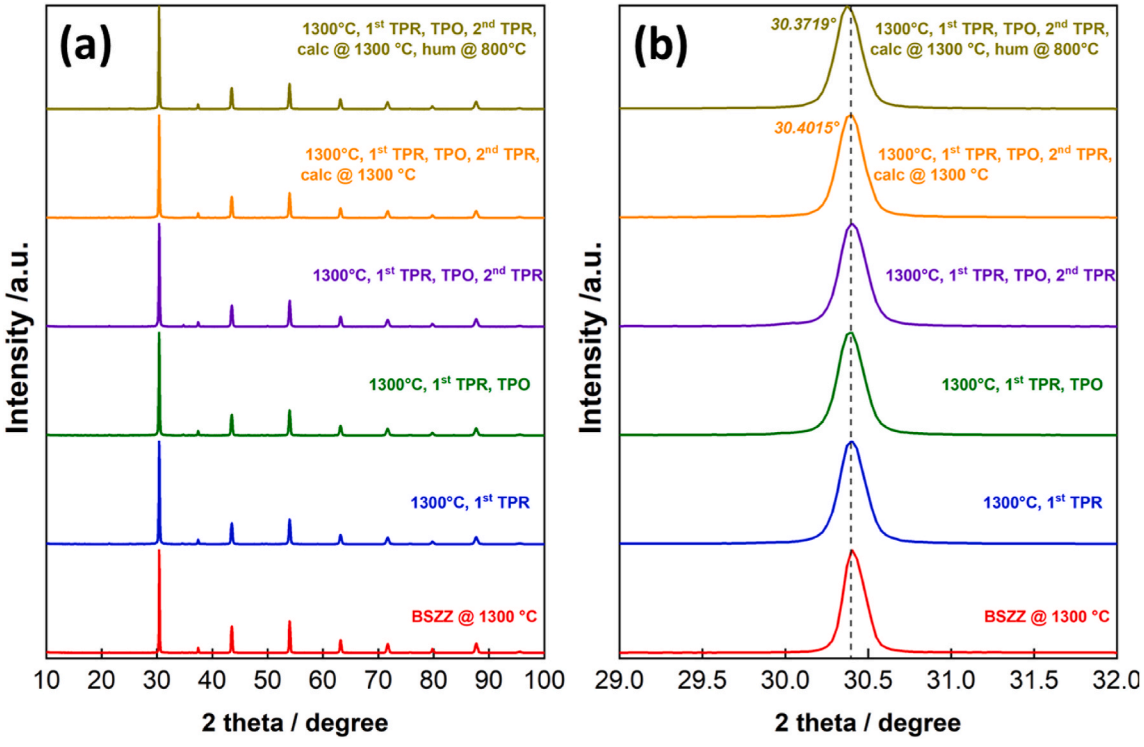

Fig. 4. XRD patterns of the BSZZ after thermochemical treatments: (a) acquisition in the entire spectral range, (b) reflections at around 30°.

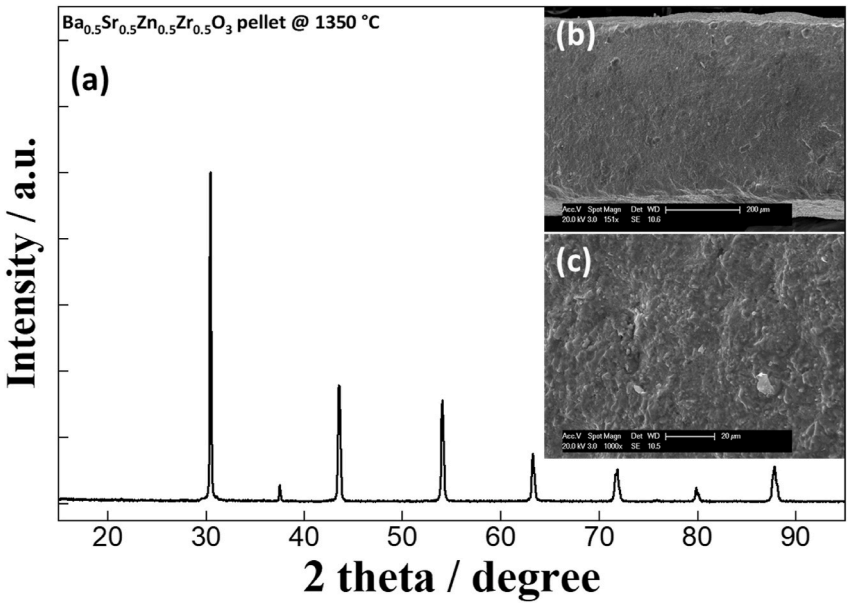

Fig. 5. XRD spectrum of the pellet treated at 1350 °C for 12 h (a) and SEM images at two magnifications (b and c) providing information about its morphology.

the Arrhenius equation, the activation energy (Ea) for BSZZ is 0.238 eV and 0.493 eV between 250 and 500 °C and 550 and 800 °C, respectively. For BZY it is 0.58 eV [31]. Clearly, the lower activation energy can be attributed to proton conductivity which, as a consequence of the moderate temperature, allow the humidification of ceramic defects to be effective. As the temperature increases, BSZZ can not hold humidity in the crystal cells and the electrical conduction become more energy-intensive, as with oxygen ions transport.

A final analysis was carried out using XPS to evaluate BSZZ's electronic state. The pellet obtained from electrochemical analysis that returned the graph in Fig. 6 was studied. Fig. 7a shows the entire energy region of the XPS spectrum with each element's position. Other elements than those constituting the phase of BSZZ were excluded in this survey analysis. Each element's analysis was carried out after aligning the carbon peak at 284.8 eV with that of adventitious carbon. Fig. 7b shows that O1s has a single band centred at 591.71 eV corresponding to oxygen in a perovskite structure [61]. According to Fig. 7c, an energy difference of 15.27 eV between the peaks of the spin-orbit components confirms that on the specimen's surface, there is only one species of Ba. In agreement with the literature, $Ba_{3d5/2}$ (779.83 eV) and $Ba_{3d3/2}$ (795.10 eV) belong to a perovskite structure [62–66]. The electronic state of Sr shown in Fig. 7d is the characteristic spin-orbit doublet of Sr_{3d}. The positions of these peaks (132.88 eV and 134.42 eV) are characteristic of Sr in the perovskite and perfectly match the spin-orbit selection rules of energy level 3d [67,68]. According to Fig. 7e, Zr_{3p} has a spin-orbit doublet feature centred at 331.93 eV and 345.53 eV, which corresponds to Zr^{4+} in zirconate-based perovskites [69,70]. Zn_{2p} is illustrated in Fig. 7f with its spin-orbit feature and sharp peaks centred at 1022.05 eV and 1045.13 eV which demonstrate its presence as an oxide in a perovskite structure [71]. Accordingly, the XPS analysis demonstrates that each element is present in a single state and phase at the surface. Thus, there is strong evidence that there is a perovskite phase, and this agrees with the XRD analysis, which showed that the phase was also very pure in bulk.

4. Conclusions

The study aimed at investigating a backbone structure based on medium entropy oxides and reducing the use of critical raw materials. A material with nominal composition $Ba_{0.5}Sr_{0.5}Zr_{0.5}Zn_{0.5}O_3$ was prepared using the Pechini method as potential electrolyte for electrochemical

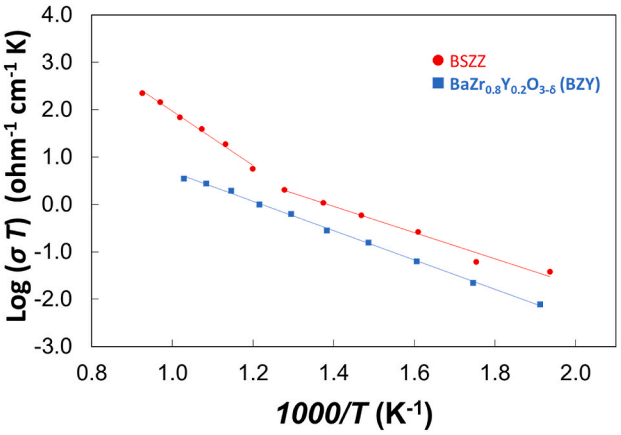

Fig. 6. Arrhenius plots for the BSZZ studied in this paper and the BZY reported by Chen et al. [33].

cells operating at intermediate temperatures; it was investigated using multiple methods in order to gain a comprehensive understanding of its characteristics, behaviour when subjected to thermal treatments, redox mechanisms. According to the preliminary results presented in this paper, the composition of this material allows for optimal phase purity at 1300 °C and an acceptable sintering already at 1350 °C, much lower than for zirconates which usually require much higher temperatures in order to achieve similar densifications. An optimization of the particle size of BSZZ and of manufacturing electrolyte supporting- or supported-cells, can allow the fabrication of complete cells within a temperature range comparable to that required by conventional devices (i.e. not less than 1400 °C). A further promising finding is that both proton conductivity and activation energy for this material are significantly higher than those of conventional yttria-doped barium zirconate (BZY). Despite the preliminary nature of the data reported in this paper, some aspects of the composition can still be improved by adding other elements, leading to materials with higher entropy, which have the potential to serve as electrolytes for electrochemical cells as proton conductive ceramics.

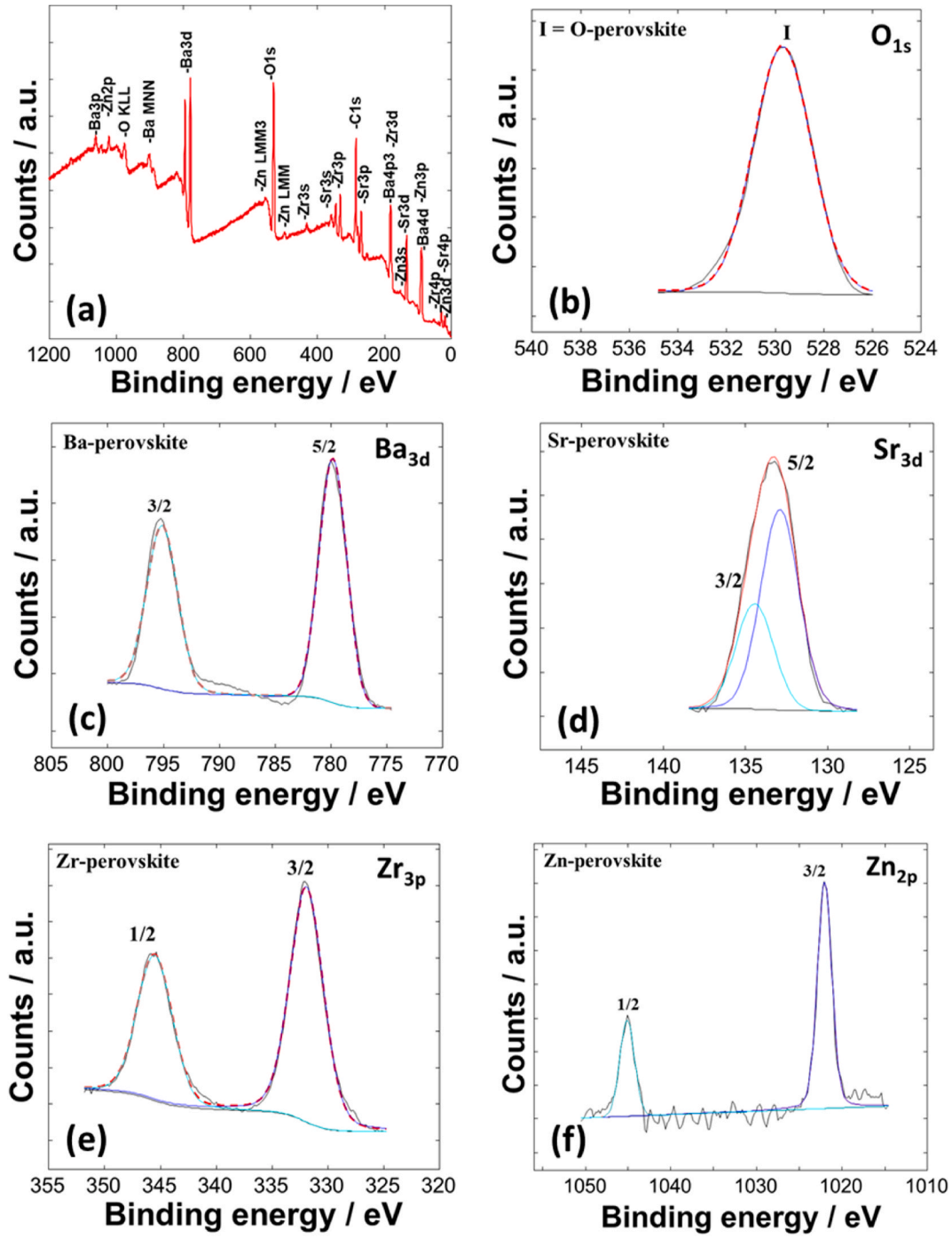

Fig. 7. XPS survey and analysis of the electronic states of BSZZ's elements.

Declaration of competing interest

The authors declare that they have no known competing financial interests or personal relationships that could have appeared to influence the work reported in this paper.

Acknowledgements

This research was funded by the European Union – NextGeneration EU from the Italian Ministry of Environment and Energy Security POR H_2 AdP MMES/ENEA with involvement of CNR and RSE, PNRR - Mission 2, Component 2, Investment 3.5 "Ricerca e sviluppo sull'idrogeno", CUP: B93C22000630006.

In addition, the authors acknowledge the MUR for funding the PRIN project SUPERH2, CUP E53D23009400006.

Dr Lo Faro acknowledges the ITELECTROLAB, the Joint lab between CNR-ITAE and IQSC-USP financed by the National Research Council of Italy (CNR) and the bilateral project "FlexPower- Solid Oxide Fuel Cell fed with Biofuel as an Electric Flexible Provider in a Distributed Grid" granted by MAECI.

VMS acknowledges the financial support of Provincia Autonoma di Trento under the project H_2@TN.

References

[1] G. Blengini, C. Latunussa, U. Eynard, C. Matos, K. Georgitzikis, C. Pavel, S. Carrara, L. Mancini, M. Unguru, D. Blagoeva, F. Mathieux, D. Pennington, Study on the EU's List of Critical Raw Materials, Final Report, 2020, 2020.

[2] C. Zhang, X. Zhao, R. Sacchi, F. You, Trade-off between critical metal requirement and transportation decarbonization in automotive electrification, Nat. Commun. 14 (2023).

[3] M. Alariqi, W. Long, P.R. Singh, A. Al-Barakani, A. Muazu, Modelling dynamic links among energy transition, technological level and economic development from the perspective of economic globalisation: evidence from MENA economies, Energy Rep. 9 (2023) 3920–3931.

[4] W.L. Filho, R. Kotter, P.G. Özuyar, I.R. Abubakar, J.H.P.P. Eustachio, N. R. Matandirotya, Understanding rare earth elements as critical raw materials, Sustainability (2023) 15.

[5] M.P. Carbonell-Blasco, C. Ruzafa-Silvestre, B. Mateu-Romero, E. Orgilés-Calpena, F. Arán-Ais, Cleaner technologies to minimise the environmental footprint of the footwear bonding process, Proc. IME C J. Mech. Eng. Sci. (2022). Here is a link to the paper: https://www.scopus.com/inward/record.uri?eid=2-s2.0-85144247702&doi=10.1177%2f09544062221140053&partnerID=40&md5=5076788cd605bbe7783ab76d8ae7f584.

[6] Z. Zhang, P. Yi, S. Hu, Y. Jin, Achieving artificial carbon cycle via integrated system of high-emitting industries and CCU technology: case of China, J. Environ. Manag. 340 (2023).

[7] M. ElSayed, A. Aghahosseini, U. Caldera, C. Breyer, Analysing the Techno-Economic Impact of E-Fuels and E-Chemicals Production for Exports and Carbon Dioxide Removal on the Energy System of Sunbelt Countries – Case of Egypt, vol. 343, Applied Energy, 2023.

[8] M. Lo Faro, D.A. Cantane, F. Naro, In the path for creating Research-to-business new opportunities on green hydrogen between Italy and Brazil, Int. J. Hydrogen Energy (2022). Here is a link to the paper: https://www.scopus.com/inward/record.uri?eid=2-s2.0-85132431146&doi=10.1016%2fj.ijhydene.2022.05.089&partnerID=40&md5=9bf6968fb65e79e15e611ef498dc048f.

[9] A. Nicita, G. Maggio, A.P.F. Andaloro, G. Squadrito, Green hydrogen as feedstock: financial analysis of a photovoltaic-powered electrolysis plant, Int. J. Hydrogen Energy 45 (2020) 11395–11408.

[10] Y. Shi, N. Cai, T. Cao, J. Zhang, High-temperature Electrochemical Energy Conversion and Storage: Fundamentals and Applications, 2017.

[11] J. González-Cobos, J.L. Valverde, A. de Lucas-Consuegra, Electrochemical vs. chemical promotion in the H2 production catalytic reactions, Int. J. Hydrogen Energy 42 (2017) 13712–13723.

[12] D. Yan, C. Mebrahtu, S. Wang, R. Palkovits, Innovative Electrochemical Strategies for Hydrogen Production: from Electricity Input to Electricity Output, vol. 62, Angewandte Chemie - International Edition, 2023.

[13] M. Lo Faro, D. La Rosa, I. Nicotera, V. Antonucci, A.S. Aricò, Electrochemical behaviour of propane-fed solid oxide fuel cells based on low Ni content anode catalysts, Electrochim. Acta 54 (2009) 5280–5285.

[14] M. Lo Faro, A.S. Arico, Electrochemical behaviour of an all-perovskite-based intermediate temperature solid oxide fuel cell, Int. J. Hydrogen Energy 38 (2013) 14773–14778.

[15] S.C. Singhal, Advances in solid oxide fuel cell technology, Solid State Ionics 135 (2000) 305–313.

[16] O. Yamamoto, Solid oxide fuel cells: fundamental aspects and prospects, Electrochim. Acta 45 (2000) 2423–2435.

[17] M. Lo, Faro, Solid Oxide-Based Electrochemical Devices: Advances, Smart Materials and Future Energy Applications, 2020.

[18] M. Noponen, P. Torri, J. Göös, D. Chade, P. Hallanoro, A. Temmo, A. Koit, E. Õunpuu, Status of Solid Oxide Fuel Cell Development at Elcogen, ECS Transactions, 2015, pp. 151–156.

[19] M. Lo Faro, A.S. Arico, Ceramic membranes for intermediate temperature solid oxide fuel cells (SOFCs): state of the art and perspectives, in: A. Gugliuzza, A. Basile (Eds.), Membranes for Clean and Renewable Power Applications, Woodhead Publ Ltd, Cambridge, 2014, pp. 237–265.

[20] S.J. Skinner, J.A. Kilner, Oxygen ion conductors, Mater. Today 6 (2003) 30–37.

[21] T. Kudo, H. Obayashi, Oxygen ion conduction of the fluorite-type $Ce_{1-x}Ln_xO_{2-x/2}$ (ln = lanthanoid element), J. Electrochem. Soc. 122 (1975) 142–147.

[22] H. Yahiro, Y. Eguchi, K. Eguchi, H. Arai, Oxygen ion conductivity of the ceria-samarium oxide system with fluorite structure, J. Appl. Electrochem. 18 (1988) 527–531.

[23] B.C.H. Steele, Oxygen transport and exchange in oxide ceramics, J. Power Sources 49 (1994) 1–14.

[24] A. Heel, A. Vital, P. Holtappels, T. Graule, Flame spray synthesis and characterisation of stabilised ZrO_2 and CeO_2 electrolyte nanopowders for SOFC applications at intermediate temperatures, J. Electroceram. 22 (2009) 40–46.

[25] B. Liu, W. Guo, F. Chen, C. Xia, Ga site doping and concentration variation effects on the conductivities of melilite-type lanthanum strontium gallate electrolytes, Int. J. Hydrogen Energy 37 (2012) 961–966.

[26] H. Iwahara, Proton conducting ceramics and their applications, Solid State Ionics 86–88 (1996) 9–15.

[27] T. Norby, Y. Larring, Concentration and transport of protons in oxides, Curr. Opin. Solid State Mater. Sci. 2 (1997) 593–599.

[28] K.D. Kreuer, On the development of proton conducting materials for technological applications, Solid State Ionics 97 (1997) 1–15.

[29] K.D. Kreuer, Aspects of the formation and mobility of protonic charge carriers and the stability of perovskite-type oxides, Solid State Ionics 125 (1999) 285–302.

[30] G. Alberti, M. Casciola, Solid state protonic conductors, present main applications and future prospects, Solid State Ionics 145 (2001) 3–16.

[31] F. Giannici, A. Longo, F. Deganello, A. Balerna, A.S. Arico, A. Martorana, Local environment of Barium, Cerium and Yttrium in $BaCe_{1-x}Y_xO_{3-\delta}$ ceramic protonic conductors, Solid State Ionics 178 (2007) 587–591.

[32] J. Lyagaeva, N. Danilov, G. Vdovin, J. Bu, D. Medvedev, A. Demin, P. Tsiakaras, A new Dy-doped $BaCeO_3$-$BaZrO_3$ proton-conducting material as a promising electrolyte for reversible solid oxide fuel cells, J. Mater. Chem. A 4 (2016) 15390–15399.

[33] M. Chen, M. Zhou, Z. Liu, J. Liu, A comparative investigation on protonic ceramic fuel cell electrolytes $BaZr_{0.8}Y_{0.2}O_{3-\delta}$ and $BaZr_{0.1}Ce_{0.7}Y_{0.2}O_{3-\delta}$ with NiO as sintering aid, Ceram. Int. 48 (2022) 17208–17216.

[34] T.S. Bjørheim, A. Kuwabara, I. Ahmed, R. Haugsrud, S. Stølen, T. Norby, A combined conductivity and DFT study of protons in $PbZrO_3$ and alkaline earth zirconate perovskites, Solid State Ionics 181 (2010) 130–137.

[35] Á. Triviño-Peláez, D. Pérez-Coll, M. Aparicio, D.P. Fagg, J. Mosa, G.C. Mather, Processing and characterisation of $BaZr_{0.8}Y_{0.2}O_{3-\delta}$ proton conductor densified at 1200 °C, J. Mater. Chem. A 10 (2022) 4428–4439.

[36] J.G. Fisher, D.H. Kim, S. Lee, D. Nguyen, J.S. Lee, Reactive sintering of $BaY_{0.1}Zr_{0.9}O_{3-\delta}$ proton conducting ceramics with CuO liquid phase sintering aid, J. Ceram. Process. Res. 14 (2013) 703–706.

[37] I. Antunes, D. Pérez-Coll, N. Nasani, H.S. Soares, G.C. Mather, J.R. Frade, D. P. Fagg, Mechanochemical processing of $BaZr_{1-y}Y_yO_{3-\delta}$ (y = 0.15, 0.20) protonic ceramic electrolytes: phase purity, microstructure, electrical properties and comparison with other preparation routes, Int. J. Hydrogen Energy 46 (2021) 13606–13621.

[38] N. Yan, Y. Zeng, B. Shalchi, W. Wang, T. Gao, G. Rothenberg, J.L. Luo, Discovery and understanding of the ambient-condition degradation of doped barium cerate proton-conducting perovskite oxide in solid oxide fuel cells, J. Electrochem. Soc. 162 (2015) F1408–F1414.

[39] N. Yan, T. Gao, W. Wang, J.L. Luo, Understanding the Aging Degradation of Doped Barium Cerate Proton Conductor in Ambient Air at Room Temperature, ECS Transactions, 2015, pp. 457–466.

[40] R.D. Carneim, T.R. Armstrong, Chemical Stability of Barium Cerate-Based High-Temperature Proton Conductors, ACS Division of Fuel Chemistry, Preprints, 2003, pp. 302–303.

[41] S. Jiang, T. Hu, J. Gild, N. Zhou, J. Nie, M. Qin, T. Harrington, K. Vecchio, J. Luo, A new class of high-entropy perovskite oxides, Scripta Mater. 142 (2018) 116–120.

[42] C. Oses, C. Toher, S. Curtarolo, High-entropy ceramics, Nat. Rev. Mater. 5 (2020) 295–309.

[43] M. Gazda, T. Miruszewski, D. Jaworski, A. Mielewczyk-Gryń, W. Skubida, S. Wachowski, P. Winiarz, K. Dzierzgowski, M. Łapiński, I. Szpunar, E. Dzik, Novel class of proton conducting materials—high entropy oxides, ACS Mater. Lett. 2 (2020) 1315–1321.

[44] C.J. Bartel, C. Sutton, B.R. Goldsmith, R. Ouyang, C.B. Musgrave, L.M. Ghiringhelli, M. Scheffler, New tolerance factor to predict the stability of perovskite oxides and halides, Sci. Adv. 5 (2019).

[45] H. Wang, R. Peng, X. Wu, J. Hu, C. Xia, Sintering behavior and conductivity study of yttrium-doped $BaCeO_3$–$BaZrO_3$ solid solutions using ZnO additives, J. Am. Ceram. Soc. 92 (2009) 2623–2629.

[46] L.S. Hagy, K. Ramos, M.V. Gelfuso, A.L. Chinelatto, A.S.A. Chinelatto, Effects of ZnO addition and microwave sintering on the properties of $BaCe_{0.2}Zr_{0.7}Y_{0.1}O_{3-\delta}$ proton conductor electrolyte, Ceram. Int. 49 (2023) 17261–17270.

[47] J. Cao, Y. Ji, Z. Shao, Perovskites for protonic ceramic fuel cells: a review, Energy Environ. Sci. 15 (2022) 2200–2232.

[48] L. Lei, J. Zhang, Z. Yuan, J. Liu, M. Ni, F. Chen, Progress report on proton conducting solid oxide electrolysis cells, Adv. Funct. Mater. 29 (2019), 1903805.

[49] D. Han, S. Uemura, C. Hiraiwa, M. Majima, T. Uda, Detrimental effect of sintering additives on conducting ceramics: yttrium-doped barium zirconate, ChemSusChem 11 (2018) 4102–4113.

[50] X. Xu, S. Tao, J.T.S. Irvine, Proton conductivity of potassium doped barium zirconates, J. Solid State Chem. 183 (2010) 93–98.

[51] J.-S. Park, J.-H. Lee, H.-W. Lee, B.-K. Kim, Effects of ZnO addition methods on proton conductivities of barium zirconate modified by ytterbium, Solid State Ionics 224 (2012) 1–5.

[52] A. Afif, N. Radenahmad, J. Zaini, A.M. Abdalla, S.M.H. Rahman, S. Eriksson, A. K. Azad, Enhancement of proton conductivity through Yb and Zn doping in $BaCe_{0.5}Zr_{0.35}Y_{0.15}O_{3-\delta}$ electrolyte for IT-SOFCs, Processing and Application of Ceramics 12 (2018) 181–189.

[53] H.S. Soares, I. Antunes, F.J.A. Loureiro, D. Pérez-Coll, M.G. Willinger, A. D. Brandão, G.C. Mather, D.P. Fagg, Effect of the addition mechanism of ZnO sintering aid on densification, microstructure and electrical properties of Ba(Zr,Y)$O_{3-\delta}$ proton-conducting perovskite, Int. J. Hydrogen Energy 46 (2021) 26466–26477.

[54] N. Nasani, Z. Shakel, F.J.A. Loureiro, B.B. Panigrahi, B.B. Kale, D.P. Fagg, Exploring the impact of sintering additives on the densification and conductivity of $BaCe_{0.3}Zr_{0.55}Y_{0.15}O_{3-\delta}$ electrolyte for protonic ceramic fuel cells, J. Alloys Compd. 862 (2021), 158640.

[55] P. Babilo, S.M. Haile, Enhanced sintering of yttrium-doped barium zirconate by addition of ZnO, J. Am. Ceram. Soc. 88 (2005) 2362–2368.

[56] S. Duran, J. Tellez, M.V. Sandoval, M.A. Macias, E. Capoen, C. Pirovano, P. Roussel, A. Niemczyk, M. Barrera Castillo, L. Mogni, L. Suescun, G.H. Gauthier, Study of $La_4BaCu_{5-x}Co_xO_{13+\delta}$ series as potential cathode materials for intermediate-temperature solid oxide fuel cell, Solid State Ionics 326 (2018) 116–123.

[57] S. Durán, N. Rangel, C. Silva, M.A. Macias, E. Capoen, C. Pirovano, A. Niemczyk, L. Suescun, P. Roussel, G.H. Gauthier, Study of $La_4BaCu_{5-x}Mn_xO_{13+\delta}$ materials as potential electrode for symmetrical-SOFC, Solid State Ionics 341 (2019), 115031.
[58] D.A.M. Monti, A. Baiker, Temperature-programmed reduction. Parametric sensitivity and estimation of kinetic parameters, J. Catal. 83 (1983) 323–335.
[59] P. Wang, D. Xu, J. Cheng, T. Hong, Proton uptake kinetics and electromotive force in $BaCo_{0.4}Fe_{0.4}Zr_{0.1}Y_{0.1}O_{3-\delta}$ cathode material with $e^-/O^{2-}/H^+$ three mobile carriers for protonic ceramic fuel cells, Ionics 27 (2021) 1185–1192.
[60] Y. Meng, J. Gao, Z. Zhao, J. Amoroso, J. Tong, K.S. Brinkman, Review: recent progress in low-temperature proton-conducting ceramics, J. Mater. Sci. 54 (2019) 9291–9312.
[61] N. Gunasekaran, S. Rajadurai, J.J. Carberry, N. Bakshi, C.B. Alcock, Surface characterization and catalytic properties of $La_{1-x}A_xMO_3$ perovskite type oxides. Part I. Studies on $La_{0.95}Ba_{0.05}MO_3$ (M = Mn, Fe or Co) oxides, Solid State Ionics 73 (1994) 289–295.
[62] J. John, S. Suresh, S.R. Chalana, V.P. Mahadevan Pillai, Effect of substrate temperature, laser energy and post-deposition annealing on the structural, morphological and optical properties of laser-ablated perovskite BaSnO3 films, Appl. Phys. A 125 (2019) 743.
[63] F. Alema, K. Pokhodnya, Dielectric properties of $BaMg_{1/3}Nb_{2/3}O_3$ doped $Ba_{0.45}Sr_{0.55}TiO_3$ thin films for tunable microwave applications, J. Adv. Dielectrics (2015), 1550030, 05.
[64] C.P. Jijil, I.M. Patil, B. Kakade, R.N. Devi, Cobalt-doped $Ba_2In_2O_5$ brownmillerites: an efficient electrocatalyst for oxygen reduction in alkaline medium, ACS Omega 3 (2018) 1710–1717.
[65] A.M. Morales Rivera, J.A. Gómez Cuaspud, C.A. Parra Várgas, M.H. Brijaldo Ramirez, Synthesis and characterization of $LaBa_2Cu_3O_{7-\delta}$ system by combustion technique, J. Supercond. Nov. Magnetism 29 (2016) 1163–1171.
[66] S. Lianwei, Z. Xianyou, XPS study on barium lanthanum magnesium niobate, J. Rare Earths 24 (2006) 310–313.
[67] P. Kulkarni, S.K. Kulkarni, A.S. Nigavekar, S.K. Agarwal, V.P.S. Awana, A. V. Narlikar, Superconductivity in Ni substituted $Bi_2Ca_1Sr_2Cu_{2-x}Ni_xO_y$, Phys. C Supercond. 166 (1990) 530–534.
[68] W.T. Hong, K.A. Stoerzinger, E.J. Crumlin, E. Mutoro, H. Jeen, H.N. Lee, Y. Shao-Horn, Near-Ambient pressure XPS of high-temperature surface chemistry in $Sr_2Co_2O_5$ thin films, Top. Catal. 59 (2016) 574–582.
[69] N. Bibi, M.Z. Hussain, S. Hussain, S. Ahmed, I. Ahmad, S. Zhang, A. Iqbal, Excellent electrochemical performance of $SrZrO_3$ nanorods as supercapacitor electrode in aqueous electrolytes, Appl. Surf. Sci. 495 (2019), 143587.
[70] A.A. Vedyagin, R.M. Kenzhin, M.Y. Tashlanov, V.O. Stoyanovskii, P.E. Plyusnin, Y. V. Shubin, I.V. Mishakov, A.V. Kalinkin, M.Y. Smirnov, V.I. Bukhtiyarov, Synthesis and study of bimetallic Pd-Rh system supported on zirconia-doped alumina as a component of three-way catalysts, Emission Control Sci. Technol. 5 (2019) 363–377.
[71] C. Battistoni, J.L. Dormann, D. Fiorani, E. Paparazzo, S. Viticoli, An XPS and Mössbauer study of the electronic properties of $ZnCr_xGa_{2-x}O_4$ spinel solid solutions, Solid State Commun. 39 (1981) 581–585.